JOURNAL OF THERMOPHYSICS AND HEAT TRANSFER
Vol. 12, No. 3, July–September 1998

Double Diffusion in a Porous Cavity Saturated with Non-Newtonian Fluid

D. Getachew,* D. Poulikakos,† and W. J. Minkowycz‡
University of Illinois at Chicago, Chicago, Illinois 60607

A numerical and theoretical study of double-diffusive natural convection within a rectangular porous cavity saturated by a non-Newtonian fluid and characterized by a power-law model is conducted. The conditions on the vertical walls are of a constant temperature and concentration. The theoretical method utilizes the pure scaling arguments to estimate, in an order-of-magnitude sense, the type of flow and the heat and mass transfer patterns that can develop in the enclosure. The results obtained using the scaling arguments are then verified by performing a series of numerical experiments. Numerical solutions for the flowfield, the temprature and concentration distributions, and the heat and mass transfer rates are obtained for a wide range of parameters. Results are presented for $50 \leq Ra \leq 500$, $0 \leq N \leq 20$, $0.1 \leq Le \leq 500$, and $0.5 \leq n \leq 1.6$. The order-of-magnitude predictions for the overall heat and mass transfer rates and their respective domains of validity are shown to be in agreement with the results produced by discrete numerical experiments.

Nomenclature

A = aspect ratio
C = concentration
c_{pf} = specific heat of the fluid
D_m = mass diffusivity
g = magnitude of the gravity vector
$\dot{g}$ = gravitational body force
H = total height of the cavity
i, j = indices
$\mathcal{K}$ = modified permeability of porous medium
K''' = effective thermal conductivity of the porous medium
L = total length of the cavity
Le = Lewis number
m = consistency index of a power-law fluid
N = buoyancy ratio
Nu = Nusselt number
n = flow-behavior index
q = heat transfer per unit depth
q_f = heat flux in the fluid phase
Ra = modified Rayleigh number for power-law fluid
S = source term
Sh = Sherwood number
T = dimensionless temperature
T_f = temperature
u, v = dimensionless velocity components
u_f, v_f = velocity components
$\boldsymbol{v}$ = velocity vector
x, y = dimensionless coordinates in the physical domain
$\bar{x}, \bar{y}$ = coordinates in the physical domain
α_m = thermal diffusivity of the porous medium
β = volumetric expansion coefficient of thermal expansion
β_c = volumetric expansion coefficient of concentration expansion
ρ_f = density of the fluid
ϕ = general dependent variable
ς = porosity
ψ = stream function

Received May 27, 1997; accepted for publication Jan. 13, 1998. Copyright © 1998 by the American Institute of Aeronautics and Astronautics, Inc. All rights reserved.

*Professor, Department of Mechanical Engineering; currently at Department of Mathematics and Computer Science, Chicago State University, Chicago, IL 60628.

†Professor, Department of Mechanical Engineering; currently at Institute for Energy Technology, Laboratory for Thermodynamics, ETH Zentrum (ML), Ch-8092 Zurich, Switzerland.

‡Professor, Department of Mechanical Engineering.

Introduction

INTEREST in studying the phenomena of momentum, mass, and heat transfer in a porous medium confined between two vertical walls maintained at different temperatures and different concentrations of a certain chemical species stems from 1) the fundamental considerations, such as to develop a better understanding of the underlying physical processes; and 2) the practical considerations, such as the migration of moisture through the air contained in fibrous insulations and grain-storage installations, and the dispersion of chemical contamination through water-saturated soil. Considerable research effort has been expanded in exploring and understanding the physics of momentum, heat, and mass transfer in these systems when the fluid exhibits simple Newtonian behavior. Indeed, books and research monographs providing a comprehensive account of developments in this area are now available.[1–3] However, relative to the research activities on Darcy flow driven by a single buoyancy effect, the work on convection driven by two simultaneous buoyancy effects is quite limited.[2,4,5] Trevisan and Bejan[2] numerically studied the flow in a square cavity with adiabatic and impermeable horizontal walls and two vertical walls maintained at different temperatures and concentrations. Using a scale analysis, the order of magnitude for the overall heat and mass transfer rates, and their respective domains of validity were predicted and assessed by an extensive series of numerical simulations. Alavyoon and co-workers[4,5] considered other boundary conditions for the cases of cooperative and opposing buoyancy forces. The problem was studied using numerical and analytical methods and scale analysis. An approximate analytical solution developed by these authors was found to be in good agreement with their numerical results. Recently, Goyeau et al.[6] studied the double-diffusive natural convection in a porous cavity using the Darcy–Brinkman model; their numerical results clearly show the influence of the Darcy number.

In all of the aforementioned investigations, the fluids saturating the porous medium were assumed to be Newtonian flu-

ids. However, not all liquids of industrial significance display Newtonian-law behavior. It is now acknowledged that most materials encountered in chemical-, biochemical-, and mineral-processing applications do not adhere to classical Newtonian behavior and are accordingly classified as non-Newtonian fluids. Clearly, it is beyond the scope of this paper to undertake a detailed discussion of non-Newtonian flow behavior per se and of the large number of rheological equations of state that have been devised to portray the behavior of real fluids. Comprehensive accounts of developments in this field are available in number of publications.[7–9]

In the literature survey, we were not able to identify any published studies on double diffusion in a porous cavity saturated with a non-Newtonian fluid. Even in the limit of convection in a rectangular porous cavity saturated with a non-Newtonian fluid driven by temperature gradient alone, the number of existing works is very limited. To this end, Bian et al.[10,11] and Getachew et al.[12] studied analytically and numerically the problem of natural convection (driven by temperature gradient) in a porous cavity saturated by a power-law fluid. They found a significant dependence of the temperature field and of the heat transfer rate on the power-law index. The problem for a simple geometry of a single vertical wall in a saturated porous medium with simultaneous heat and mass transfer from the wall was solved via scale analysis and numerical simulations by Rastogi and Poulikakos.[13] They showed that the buoyancy-driven flow that coats the wall can have, depending on the order of magnitude of the buoyancy ratio and the Lewis number, one of the four two-layer structures. Their results documented that the variation of the wall temperature and concentration, necessary to yield a constant heat and species flux at the wall, depend on the power-law index.

Considering the research contributions reviewed in the preceding text, the objective of the analytical and numerical work of the present study is to predict the characteristics of steady natural convection heat and mass transfer of non-Newtonian fluids in an enclosed porous medium. Scaling analysis is performed to identify the various flow, heat transfer, and mass transfer regimes. Also, detailed numerical solutions of the governing equations using a control volume-based finite difference method are obtained for a large range of values of the governing parameters. The results presented here are relevant to an adequate understanding of the general flow and heat and mass transfer characteristics of non-Newtonian flows in a porous cavity.

Formulation of the Problem

Consider the two-dimensional system defined in Fig. 1. The porous medium is assumed to be saturated with a purely viscous non-Newtonian fluid that is of the Ostwald de Waele power-law type. Horizontal temperature and concentration differences are specified between the vertical walls (T_1 and C_1 at the left wall and T_0 and C_0 at the right wall). The top and the bottom walls are considered to be perfectly insulated. The coordinate system is defined so that the vertical axis points vertically upward in the direction opposite to the gravity vector of magnitude g. The x axis is horizontal. The combined effect of temperature and species concentration nonuniformities in the fluid-saturated porous medium causes density changes to the fluid in the cavity and leads to a buoyancy-driven circulation. Employing the Boussinesq approximation, the density variation can be expressed as

$$\rho_f \cong \rho_0[1 - \beta_f(T - T_0) - \beta_c(C - C_0)] \tag{1}$$

where the zero subscript indicates the property of the mixture in a reference state and β_f is the volumetric thermal expansion coefficient. The resulting flow is treated as steady, laminar, and two dimensional. Furthermore, in the formulation of the problem, it has been assumed that 1) the fluid properties are constant, except for the density variation in producing the buoyancy force; 2) the viscous drag and inertia terms are neglected; 3) the velocity slip at the bounding surfaces is permitted; and 4) the viscous heat dissipation, the compression work, and the heat generation are assumed to be negligible. The equations that account for the conservation of mass, energy, constituent and momentum, according to the preceding assumptions, are

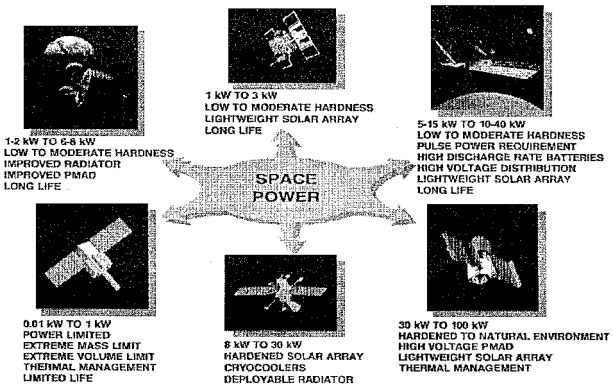

Fig. 1 Schematic diagram of the physical model and the coordinates system.

$$\frac{\partial u_f}{\partial \bar{x}} + \frac{\partial v_f}{\partial \bar{y}} = 0 \tag{2}$$

$$u_f \frac{\partial T_f}{\partial \bar{x}} + v_f \frac{\partial T_f}{\partial \bar{y}} = \frac{\partial}{\partial \bar{x}}\left(\alpha_m \frac{\partial T_f}{\partial \bar{x}}\right) + \frac{\partial}{\partial \bar{y}}\left(\alpha_m \frac{\partial T_f}{\partial \bar{y}}\right) \tag{3}$$

$$u_f \frac{\partial C}{\partial \bar{x}} + v_f \frac{\partial C}{\partial \bar{y}} = \frac{\partial}{\partial \bar{x}}\left(D_m \frac{\partial C}{\partial \bar{x}}\right) + \frac{\partial}{\partial \bar{y}}\left(D_m \frac{\partial C}{\partial \bar{y}}\right) \tag{4}$$

$$\frac{\partial p}{\partial \bar{x}} = -\frac{\varepsilon}{K}|\boldsymbol{v}_f|^{n-1}u_f \tag{5}$$

$$\frac{\partial p}{\partial \bar{y}} - \rho_0 g[1 - \beta_f(T_f - T_0) - \beta_c(C - C_0)] = -\frac{\varepsilon}{K}|\boldsymbol{v}_f|^{n-1}v_f \tag{6}$$

Next, the elimination of p between the two equations yields

$$\frac{\varepsilon}{K}\frac{\partial}{\partial \bar{y}}(|\boldsymbol{v}_f|^{n-1}u_f) - \frac{\varepsilon}{K}\frac{\partial}{\partial \bar{x}}(|\boldsymbol{v}_f|^{n-1}v_f) = -\rho_f g\beta_f \frac{\partial T_f}{\partial \bar{x}} - \rho_f g\beta_c \frac{\partial C}{\partial \bar{x}} \tag{7}$$

where

$$\varepsilon = \frac{2\mu}{8^{(n+1)/2}(K\varsigma)^{(n-1)/2}\left(\dfrac{n}{1+3n}\right)^n}, \qquad |\boldsymbol{v}_f| = (u_f^2 + v_f^2)^{1/2} \tag{8}$$

The temperature and the concentration gradients on the right-hand side of Eq. (7) account for the two buoyancy effects that drive the flow and heat and mass transfer processes. In the preceding equations, ε is a parameter in the power-law model given by Pascal,[14] T represents the local equilibrium temperature of the fluid and the porous matrix, and C is the concentration of the constituent per unit volume of the porous medium (solid and fluid). The relevant hydrodynamic and thermal boundary conditions, shown in Fig. 1, are

$$u_f = 0, \qquad T = T_1, \qquad C = C_1 \quad \text{at} \quad \bar{x} = 0 \tag{9}$$

$$u_f = 0, \qquad T = T_0, \qquad C = C_0 \quad \text{at} \quad \bar{x} = L \tag{10}$$

$$v_f = 0, \qquad \frac{\partial T}{\partial \bar{y}} = 0, \qquad \frac{\partial C}{\partial \bar{y}} = 0 \quad \text{at} \quad \bar{y} = 0, \qquad H \tag{11}$$

The flow, concentration, and temperature fields in the porous cavity can be obtained by solving Eqs. (2–4) and Eq. (7), subject to the boundary conditions given by Eqs. (9–11).

In the following sections we develop the analytical and numerical solutions. The analytical solution utilizes pure scaling arguments[1,15] to estimate in an order-of-magnitude sense the type of flow and the heat and mass transfer regimes that can exist; whereas for the numerical solutions, a control volume-based finite difference scheme has been used to discretize the conservation equations, and a power-law scheme has been used to evaluate the finite difference coefficients. The detailed description of the method may be found in Ref. 12. The implementation of these two methods for solving the aforementioned problem will be discussed in the following sections.

Scale Analysis

To enhance the interpretation of the numerical results of this study, a scaling analysis is performed that shows the many distinct flow and heat and mass transfer regimes that can exist. For the case where the fluid is Newtonian ($n = 1$), Trevisan and Bejan[2] identified these regimes on the basis of numerical experiments and scale analysis. As pointed out in Ref. 2, in view of the many dimensionless parameters that govern the natural-convection phenomenon, the task of selecting the best cases for direct numerical simulation and to assess the effect of each of these dimensionless parameters is complicated. Thus, following the work presented in Ref. 2, the natural convection flow under consideration may be divided into two limiting classes: 1) flows dominated by the buoyancy effect because of temperature changes, i.e., heat transfer-driven flow; and 2) flows dominated by the buoyancy effect dominated by density changes associated with the concentration variation, i.e., mass transfer-driven flow.

Heat Transfer-Driven Flows

The scale equivalence for the mass, energy, and momentum equations in a vertical thermal boundary-layer region of thickness δ_T and height H are taken as

$$\frac{u}{v} \sim \frac{\delta_T}{H} \tag{12}$$

$$\frac{v}{H}\,\Delta T\left(\frac{u}{v}\frac{H}{\delta_T} + 1\right) \sim \alpha_m \frac{\Delta T}{\delta_T^2}\left[1 + \left(\frac{\delta_T}{H}\right)^2\right] \tag{13}$$

$$\frac{v}{\delta_T}\left[v\sqrt{\left(\frac{\delta_T}{H}\right)^2 + 1}\right]^{n-1}\left[\left(\frac{\delta_T}{H}\right)^2 - 1\right] \sim -\frac{\rho g \beta \mathcal{K}}{\varepsilon}\frac{\Delta T}{\delta_T} \tag{14}$$

Because $\delta_T \times H$ is a boundary layer, we may assume $\delta_T << H$. Based on the preceding equations, solving the system [Eqs. (12–14)] for the three unknowns, the scales for the vertical boundary layers in the cavity are

$$v \sim \frac{\alpha_m}{H}(Ra)^{1/n} \tag{15}$$

$$\delta_T \sim H(Ra)^{-(1/2n)} \tag{16}$$

$$u \sim \frac{\alpha_m}{H}(Ra)^{1/2n} \tag{17}$$

where the modified Darcy–Rayleigh number for a non-Newtonian flow, based on the height of the cavity, is defined as

$$Ra = \frac{\rho g \beta_f \mathcal{K} H^n \Delta T}{\varepsilon \alpha_m^n}$$

Although in the present limit the flow is driven by the temperature gradient, a mass transfer occurs because the constituent in the mixture is carried along with the flow and, at the same time, is rich in the species-diluted mixture. Thus, to obtain the scale equivalence of the constituent equation, we denote the concentration boundary-layer thickness by δ_c. In the flow region of thickness δ_c and height H, the concentration equation [Eq. (4)] requires

$$\frac{v}{H}\,\Delta C\left(\frac{u}{v}\frac{H}{\delta_C} + 1\right) \sim D_m \frac{\Delta C}{\delta_C^2}\left[1 + \left(\frac{\delta_C}{H}\right)^2\right] \tag{18}$$

Assuming $\delta_C << H$ and using Eq. (12), Eq. (18) takes the form

$$\delta_C(\delta_T + \delta_C) \sim \frac{H^2}{Le}(Ra)^{-(1/n)} \tag{19}$$

In the heat transfer-driven flow, the velocity boundary layer is δ_T thick and the concentration boundary layer is δ_C thick. Thus, $\mathcal{O}(\delta_T + \delta_C)$ should represent the vertical boundary-layer region, where the fluid flows vertically as a result of the thermal gradient and, at the same time, has a high concentration of the constituent. The implication of the preceding statement is that the order of the quantity $(\delta_T + \delta_C)$ depends on the relative magnitude of δ_T and δ_C. This leads to the following two possibilities:

$$(\delta_T + \delta_C) \sim \begin{cases} \mathcal{O}(\delta_T) & \text{if} \quad \delta_T < \delta_C \quad \text{Case 1} \\ \mathcal{O}(\delta_C) & \text{if} \quad \delta_T > \delta_C \quad \text{Case 2} \end{cases} \tag{20}$$

Based on the preceding argument, Eq. (19) yields the following scales for δ_C:

For Case 1:

$$\delta_C \sim HLe^{-1}(Ra)^{(-1)/2n} \tag{21a}$$

For Case 2:

$$\delta_C \sim HLe^{-(1/2)}(Ra)^{(-1)/2n} \tag{21b}$$

The scaling analysis presented in the preceding text may be utilized to set the criteria for distinguishing the distinct regimes that are possible when the buoyancy effect is caused mainly by temperature gradients. To this effect we will focus on two limiting cases. First, consider the criterion for having distinct thermal boundary layers ($\delta_T << L$). For this case Eq. (16) implies that

$$(L/H)(Ra)^{1/2n} >> 1 \tag{22}$$

Furthermore, from the scales of δ_C and δ_T given by Eqs. (16) and (21), it can be shown that

$$\frac{\delta_C}{\delta_T} \sim \begin{cases} Le^{-1} & \text{when} \quad \delta_T << \delta_C \\ Le^{-(1/2)} & \text{when} \quad \delta_T >> \delta_C \end{cases} \tag{23}$$

which can be used to set the following criteria:

$$Le >> 1 \quad \text{when} \quad \delta_T >> \delta_C \tag{24}$$

$$Le << 1 \quad \text{when} \quad \delta_T << \delta_C \tag{25}$$

In addition, for the case where $\delta_C >> \delta_T$, although we assumed that $\delta_T << L$, it is possible that the concentration boundary layers can be distinct for $\delta_C << L$ or not distinct when $\delta_C \sim L$. For the case where $\delta_C << L$, Eq. (21a) yields the following criterion:

$$Le(L/H)Ra^{1/2n} >> 1 \tag{26}$$

The second limit of interest is the case when the thermal boundary layers are not distinct. For this situation, the scaling laws obtained from the mass and the momentum equations in the $L \times H$ region are

$$(u/L) \sim (v/H) \tag{27}$$

$$v^n \sim (\rho g \beta_f \mathcal{K}/\varepsilon)\Delta T \tag{28}$$

from which we get the following scales for (u, v):

$$u \sim (L/H)(\alpha_m/H)(Ra)^{1/n} \tag{29}$$

$$v \sim (\alpha_m/H)(Ra)^{1/n} \tag{30}$$

From the energy equation and employing these vertical scales, it can be shown that

$$\frac{\text{vertical convection}}{\text{lateral diffusion}} = \frac{v\Delta T/H}{\alpha_m \Delta T/L^2} \sim \left(\frac{L}{H}\right)^2 (Ra)^{1/n} \tag{31}$$

Absence of a distinct thermal boundary layer implies that lateral diffusion is greater than vertical convection. Thus, Eq. (31) yields the following criterion:

$$(L/H)(Ra)^{1/2n} << 1 \tag{32}$$

Also, employing the result obtained for case 2 [see Eq. (21b)], it can be shown that

$$(L/H)Le^{1/2}(Ra)^{1/2n} >> 1 \tag{33}$$

In conclusion, for the heat transfer-driven flow, the results presented in this section show that, for the given values of the aspect ratio and power-law index, the flow regimes occupy well-defined regions in the two-dimensional Le–Ra domain. For a square cavity, the logarithmic plot of this domain is depicted in Fig. 2. The effect of the fluid motion on the overall heat and mass transfer rates was calculated by computing the diffusion-referenced Nusselt and Sherwood numbers defined, respectively, by

$$\begin{aligned} Nu &= Q/[K'''H(T_1 - T_0)/L] \\ Sh &= j'/[D_m H(C_1 - C_0)/L] \end{aligned} \tag{34}$$

where Q and j' are the heat and mass transfer rates. The scale equivalent of the Nusselt and the Sherwood numbers, respectively, are

$$Nu \sim (L/\delta_T), \qquad Sh \sim (L/\delta_C) \tag{35}$$

Employing these results, the main conclusions of the scale analysis regarding the overall heat and mass transfer rates are shown for each subdomain in Fig. 2.

Mass Transfer-Driven Flows

For the case where the flow is driven by buoyancy primarily because of concentration gradients, the order-of-magnitude equivalent of the mass, constituent, and momentum equations are

$$\frac{u}{v} \sim \frac{\delta_C}{H} \tag{36}$$

$$\frac{v}{\delta_C}\left[v\sqrt{\left(\frac{\delta_C}{H}\right)^2 + 1}\right]^{n-1}\left[\left(\frac{\delta_C}{H}\right)^2 - 1\right] \sim -\frac{\rho g \beta_C \mathcal{K}}{\varepsilon}\frac{\Delta C}{\delta_C} \tag{37}$$

$$\frac{v}{H}\Delta C\left(\frac{u}{v}\frac{H}{\delta_C} + 1\right) \sim D_m \frac{\Delta C}{\delta_C^2}\left[1 + \left(\frac{\delta_C}{H}\right)^2\right] \tag{38}$$

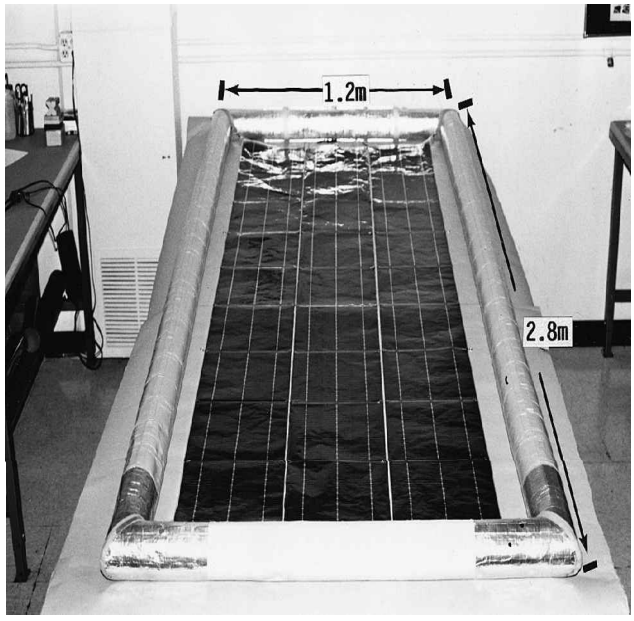

Fig. 2 Flow regimes when the buoyancy is caused by temperature gradient.

Equations (36–38) imply that, in the $\delta_C \times H$ region, the scales for the vertical boundary layers for the mass transfer-driven flow are

$$v \sim \left(\frac{\rho g \mathcal{K} \beta_C \Delta C}{\varepsilon}\right)^{1/n} \Rightarrow v \sim \frac{\alpha_m}{H}(RaN)^{1/n} \tag{39}$$

$$\delta_C^2 \sim \frac{D_m}{H}\left(\frac{\rho g \mathcal{K} \beta_C \Delta C}{\varepsilon}\right)^{(-1)/n} \Rightarrow \delta_C \sim HLe^{-(1/2)}(RaN)^{-(1/2n)} \tag{40}$$

$$u \sim \frac{\delta_C}{H} v \Rightarrow u \sim \frac{\alpha_m}{H} Le^{-(1/2)}(RaN)^{1/2n} \tag{41}$$

To obtain the scale equivalent of the energy equation, we let δ_T denote the thermal boundary-layer thickness, or

$$\frac{v}{H}\Delta T\left(\frac{u}{v}\frac{H}{\delta_T} + 1\right) \sim \alpha_m \frac{\Delta T}{\delta_T^2}\left[1 + \left(\frac{\delta_T}{H}\right)^2\right] \tag{42}$$

Assuming that $\delta_T << H$

$$\delta_T(\delta_T + \delta_C) \sim H^2(RaN)^{(-1)/n} \tag{43}$$

Using the fact that in the mass transfer-driven flow the velocity boundary layer is δ_C thick and the temperature boundary layer is δ_T thick, and following the arguments presented in the preceding section, it can be shown that for the case where $\delta_T > \delta_C$

$$\delta_T \sim HLe^{1/2}(RaN)^{-(1/2n)} \tag{44}$$

whereas, for the case where $\delta_T < \delta_C$

$$\delta_T \sim H(RaN)^{-(1/2n)} \tag{45}$$

Figure 3 shows the Le vs $Ra|N|$ plane and the relative position of all the flow regimes possible for the mass transfer-driven flow. Figure 3 also shows the scaling predictions concerning the overall heat and mass transfer rates in the form of Nu and Sh.

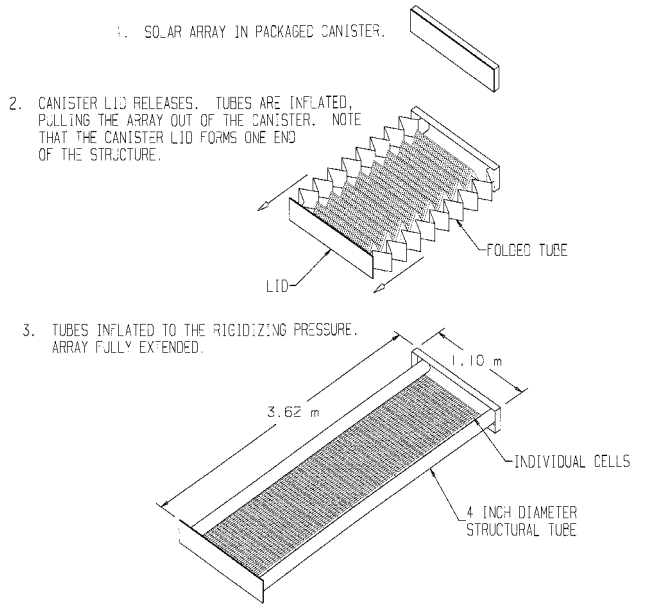

Fig. 3 Flow regimes when the buoyancy is caused by concentration gradient.

Numerical Method

Nondimensionalization

The numerical solution is aided by rewriting Eqs. (2–4) and Eq. (7) in nondimensional forms by defining a new set of variables given by

$$x = \frac{\bar{x}}{H}, \qquad y = \frac{\bar{y}}{H}, \qquad T = \frac{(T_f - T_c)}{(\Delta T)}$$

$$C = \frac{(C_f - C_0)}{(\Delta C)}, \qquad u = \frac{u_f \varepsilon \alpha^{n-1}}{\rho_f g \mathcal{K} \beta_f \Delta T L^{n-1}} \tag{46}$$

$$v = \frac{v_f \varepsilon \alpha^{n-1}}{\rho_f g \mathcal{K} \beta_f \Delta T L^{n-1}}, \qquad \psi = \frac{\psi_f \varepsilon \alpha^{n-1}}{\rho_f g \mathcal{K} \beta_f \Delta T L^{n}}$$

where ψ_f is the stream function [$u_f = (\partial\psi_f/\partial\bar{y})$, $v_f = -(\partial\psi_f/\partial\bar{x})$]. Using these transformations the dimensionless governing equations for the case of Darcy's flow are

$$\left(\frac{L}{H}\right)^n Ra \left[\frac{\partial(uT)}{\partial x} + \frac{\partial(vT)}{\partial y}\right] = \frac{\partial^2 T}{\partial x^2} + \frac{\partial^2 T}{\partial y^2} \tag{47}$$

$$\left(\frac{L}{H}\right)^n LeRa \left[\frac{\partial(uC)}{\partial x} + \frac{\partial(vC)}{\partial y}\right] = \frac{\partial^2 C}{\partial x^2} + \frac{\partial^2 C}{\partial y^2} \tag{48}$$

$$\left(\frac{L}{H}\right)^{n^2-n} Ra^{n-1} \left[\frac{\partial}{\partial x}\left(|\boldsymbol{v}|^{n-1}\frac{\partial\psi}{\partial x}\right) + \frac{\partial}{\partial y}\left(|\boldsymbol{v}|^{n-1}\frac{\partial\psi}{\partial y}\right)\right] = -\frac{\partial T}{\partial x} - N\frac{\partial C}{\partial x} \tag{49}$$

The dimensionless boundary conditions become

$$u = 0, \quad \psi = 0, \quad T = 1, \quad C = 1 \quad \text{at} \quad x = 0 \tag{50}$$

$$u = 0, \quad \psi = 0, \quad T = 0, \quad C = 0 \quad \text{at} \quad x = 1 \tag{51}$$

$$v = 0, \quad \psi = 0, \quad \frac{\partial T}{\partial y} = 0, \quad \frac{\partial C}{\partial y} = 0 \quad \text{at} \quad y = 0, \quad y = \frac{H}{L} \tag{52}$$

Equations (47–49), together with the boundary conditions given by Eqs. (50–52), complete the problem definition. The solution is dependent on Ra, the N, Le, the power-law index n, and the aspect ratio L/H. These dimensionless groups are given by

$$Ra = \frac{\rho g \beta_f \mathcal{K} H^n \Delta T}{\varepsilon \alpha_m^n}, \quad N = \frac{\beta_c \Delta C}{\beta_f \Delta T}, \quad Le = \frac{\alpha_m}{D_m}, \quad |\boldsymbol{v}| = \sqrt{u^2 + v^2} \tag{53}$$

The average heat and mass fluxes at the walls are given in dimensionless terms by the Nusselt and the Sherwood numbers, defined, respectively, as

$$Nu = \frac{1}{A}\int_0^A \frac{\partial T}{\partial x}\,dy, \qquad Sh = \frac{1}{A}\int_0^A \frac{\partial C}{\partial x}\,dy \tag{54}$$

Numerical Experiments

To perform the numerical experiments, a control volume-based finite difference scheme has been used to discretize the conservation equations.[14] The discretization equations (which are the algebraic counterparts of the foregoing differential equations), are derived by integrating the governing differential equations over a control volume. The heat and mass fluxes across the boundaries of each control volume were calculated using the power-law scheme. The discretized equations were then treated as a set of linear equations and solved, iteratively, using the line-by-line method idea proposed by Patankar.[16] An 82×82 uniform grid was found to accurately model the solution fields described in the results for most of the cases considered. The detailed description of this procedure is given in Refs. 12 and 16–18.

Two criteria were applied in this study: 1) pointwise convergence for the stream function, temperature, and concentration fields; and 2) the global convergence for the total heat and mass transfer rate at the hot wall. The criterion used for iterative convergence was

$$\frac{\sum_{i,j} |(\phi_{i,j})_{\text{new}} - (\phi_{i,j})_{\text{old}}|}{\sum_{i,j} |(\phi_{i,j})_{\text{new}}|} < r_f \tag{55}$$

whereas, for the global convergence we used the conditions that

$$\left|\frac{(Nu)_{x=1} - (Nu)_{x=0}}{(Nu)_{x=1} + (Nu)_{x=0}}\right| < 0.01, \qquad \left|\frac{(Sh)_{x=1} - (Sh)_{x=0}}{(Sh)_{x=1} + (Sh)_{x=0}}\right| < 0.01 \tag{56}$$

where ϕ stands for ψ, T, or C, and r_f has been taken as 10^{-4}.

Numerical Accuracy Test

To validate the code we compared the present results to those reported in the literature for the limiting case of Newtonian fluid flow. To our knowledge, the only available results

Table 1 Comparison of Nusselt and Sherwood numbers between the present results and those reported in Refs. 2 and 6

				Ref. 2		Ref. 6	
Ra	*Le*	*Nu*	*Sh*	*Nu*	*Sh*	*Nu*	*Sh*
5000	1.00	1.97	1.97	2.02	2.02	1.98	1.98
	10.00	1.97	8.63	2.02	9.69	1.98	8.78
100.00	1.00	3.07	3.07	3.27	3.27	3.11	3.11
	10.00	3.07	13.10	3.27	16.69	3.11	13.25
	50.00	3.07	28.90	——	——	3.11	29.72
400.00	1.00	7.58	7.58	9.69	9.69	7.77	7.77
	10.00	7.58	27.90	9.69	30.73	7.77	28.41

in this configuration have been proposed by Trevisan and Bejan[2] and Goyeau et al.[6] The results of these comparisons are given in Table 1, where the numerical predictions of the overall Nusselt numbers and the Sherwood numbers obtained at the hot wall, for various values of Ra and Le, along with the corresponding numerical results reported in Refs. 2 and 6, are presented.

It may be seen from the results that the agreement with the reference solutions available in Ref. 6 is excellent. However, some discrepancy between the present results and those of Ref. 2, where the discordance is particularly significant at the higher values of the Rayleigh number, is observed. The conjecture stated in Ref. 6, i.e., that the results proposed in Ref. 2 somewhat overestimate the Nusselt and Sherwood numbers, seems to be accurate. A comparison of the present results and those of Goyeau et al.,[6] and Trevisan and Bejan,[2] with the analytical results reported by Walker and Homsy,[19] indicates that the numerical results based on the present algorithm and those reported in Ref. 6 also agreed well with those obtained in Ref. 19.

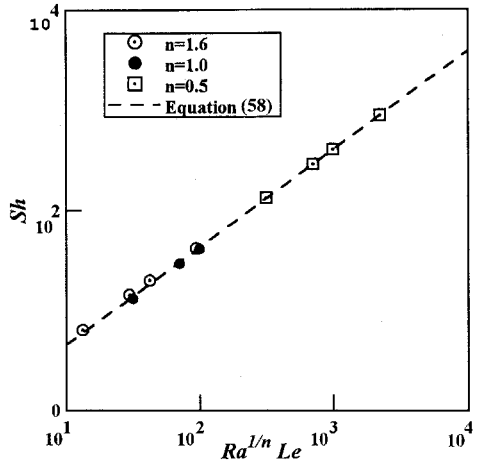

Fig. 4 Mass transfer by thermal and natural convection ($N = 0$).

Results and Discussion

The approximate solutions developed in the scale-analysis section are valid asymptotically in the limit of high- and low-buoyancy ratios. From the scale-analysis results, we see that the possible flow regimes occupy well-defined regions in the two-dimensional domain (see Figs. 2 and 3). These flow regimes are identified as I, II, III, IV, and V. Each of the regimes has its own characteristics and depends on the parameters associated with the problem: Ra, Le, n, and N. By varying only one of these parameters, while fixing the others, we may observe a change in the flow regions. One interesting feature revealed by the scale analysis is that for both the heat transfer-driven flow and the mass transfer-driven flow, the variation of the power-law index, for fixed values of Ra and Le, also changes the flow structure. For example, Fig. 2 shows the effect of n on the possible flow regimes for the heat transfer-driven flow; whereas Fig. 3 shows the effect on the mass transfer-driven flow. On each subdomain (see Figs. 2 and 3), the main conclusions of scale analysis regarding the overall heat and mass transfer rates are clearly stated.

In this section numerical solutions of the complete governing equations are presented. These solutions, which can handle both the heat transfer-driven flows and the mass transfer-driven flows, will be used to determine the accuracy of the results predicted using scale analyses. The range of parameters that has been examined in this study concern the $N > 0$ domain (cooperating buoyancy forces). The values of N have been

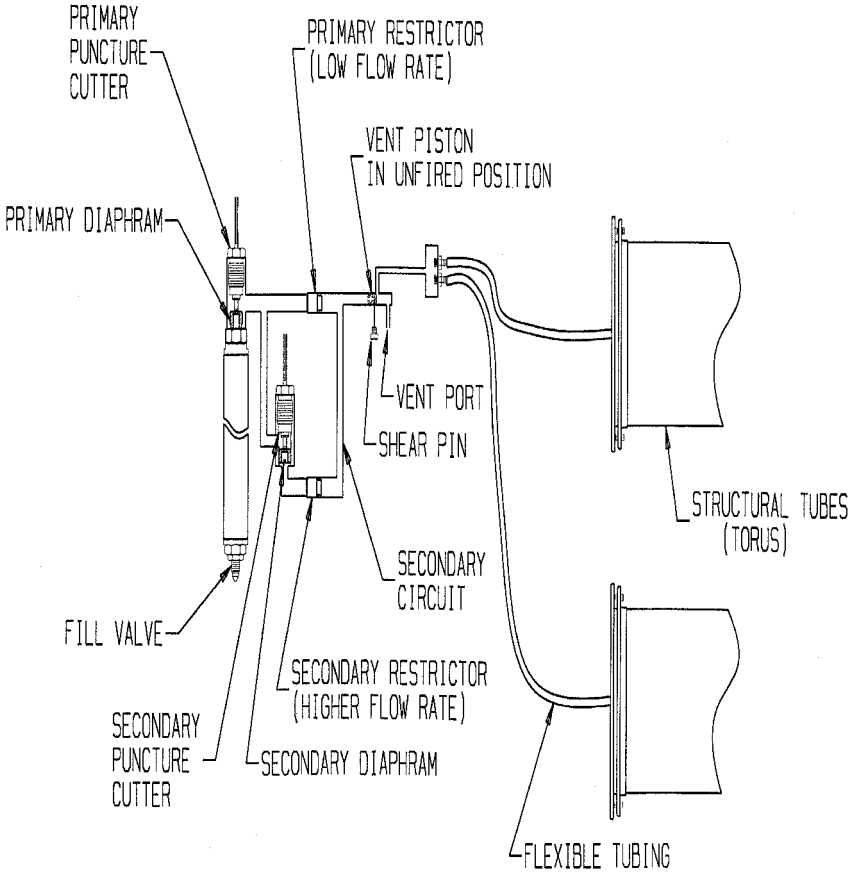

Fig. 5 Influence of the power-law index on the patterns of a) streamlines, b) isotherms, and c) concentration lines (for $Ra = 100$, $Le = 10$, and $N = 0$).

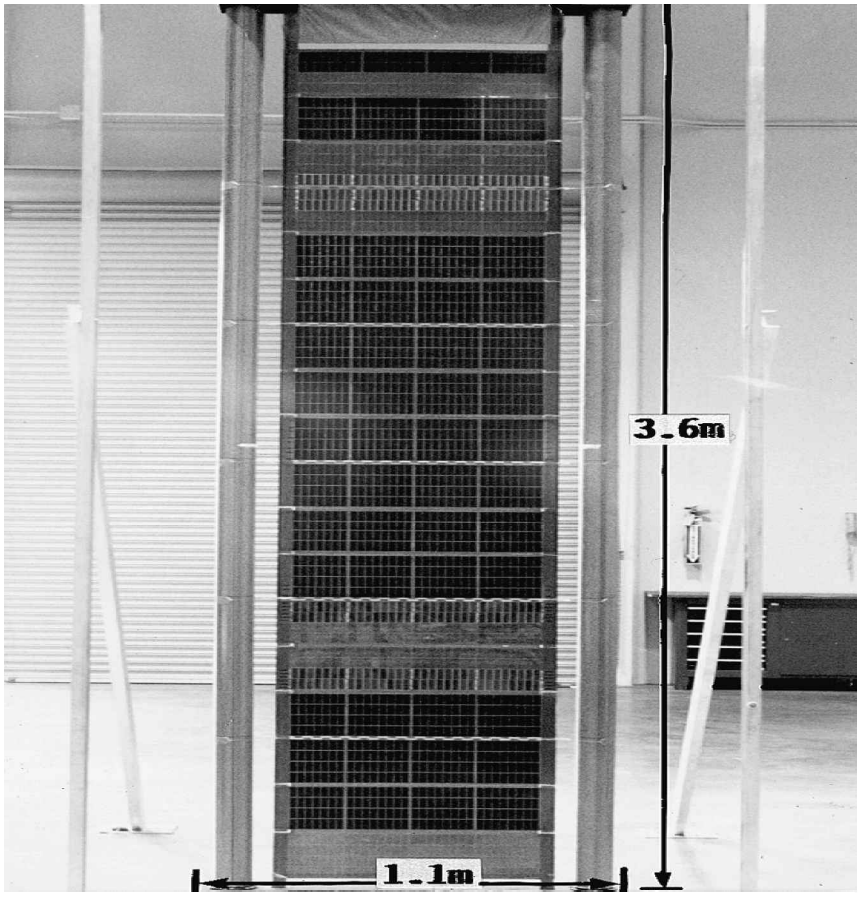

Fig. 6 Influence of the power-law index on the pattern of a) streamlines, b) isotherms, and c) concentration lines (for $Ra = 100$, $Le = 0.1$, and $N = 0$).

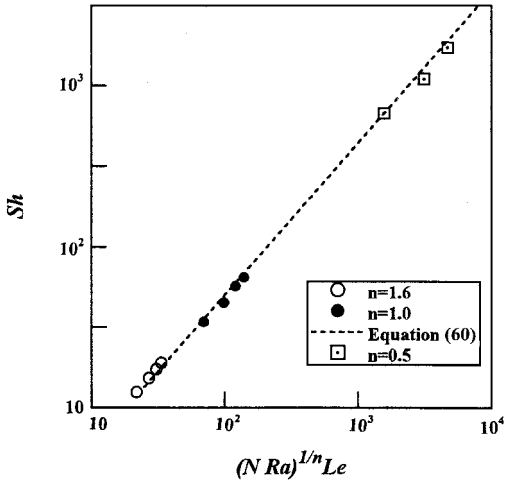

Fig. 7 Mass transfer as a function of the dimensionless group $(NRa)^{1/n}Le$.

taken in the range between 0 and 20, where $N = 0$ corresponds to the heat transfer-driven flow, and $N \geq 1$ corresponds to mass transfer-driven flow. All simulations are performed in the range $0.1 \leq Le \leq 500$ and $10 \leq Ra \leq 500$. The influence of the power-law index has been analyzed by varying the values of n from 0.5 to 1.6, which includes shear-thinning ($n < 1$) and shear-thickening ($n > 1$) fluids. With a view to illustrate the crucial features and the domain of the validity of the scaling-analysis solutions, a representative selection of the results is presented in Figs. 4–10.

Mass Transfer Results

Numerical results for shear-thickening fluids ($n > 1$) and shear-thinning fluids ($n < 1$) for a range of Le and Ra values, corresponding for the heat transfer-driven flow, are displayed in Table 2. The numerical results show that the Sherwood number clearly increases with increasing Le and Ra. This is in agreement with the analytical results of the scale analysis [from Eq. (35)]

$$Sh \sim (L/H)(\sqrt[n]{RaLe})^{1/2} \tag{57}$$

As a first test of the validity of the scaling results and using the data presented in Tables 1 and 2, the numerical results obtained on the entire range of parameters given in the tables are displayed in Fig. 4 as a function of $[(Ra)^{1/n}Le]$. A regression of the results leads to the following correlation:

$$Sh = 0.537(\sqrt[n]{RaLe})^{0.485} \tag{58}$$

where the exponent is in good agreement with the value 0.5 assessed by the scale analysis.

To show the effect of n on the flow structure, the results from the scaling analysis that corresponds to the shear-thinning fluids ($n < 1$) are plotted with the solid lines in Fig. 2 to be distinguishable from shear-thickening fluids ($n > 1$). From this figure it is evident that if the $Le > 1$ and $Ra > 1$ (regime I), the scale analysis results show boundary-layer structures for both shear-thinning and shear-thickening fluids; whereas, when $Le < 1$ and $Ra > 1$ (regime II), there exists a region where the flow experiences a boundary-layer structure when $n < 1$ and diffusion-dominated flow when $n > 1$.

The validity of the aforementioned scaling results is confirmed by the observation of the flow, temperature, and con-

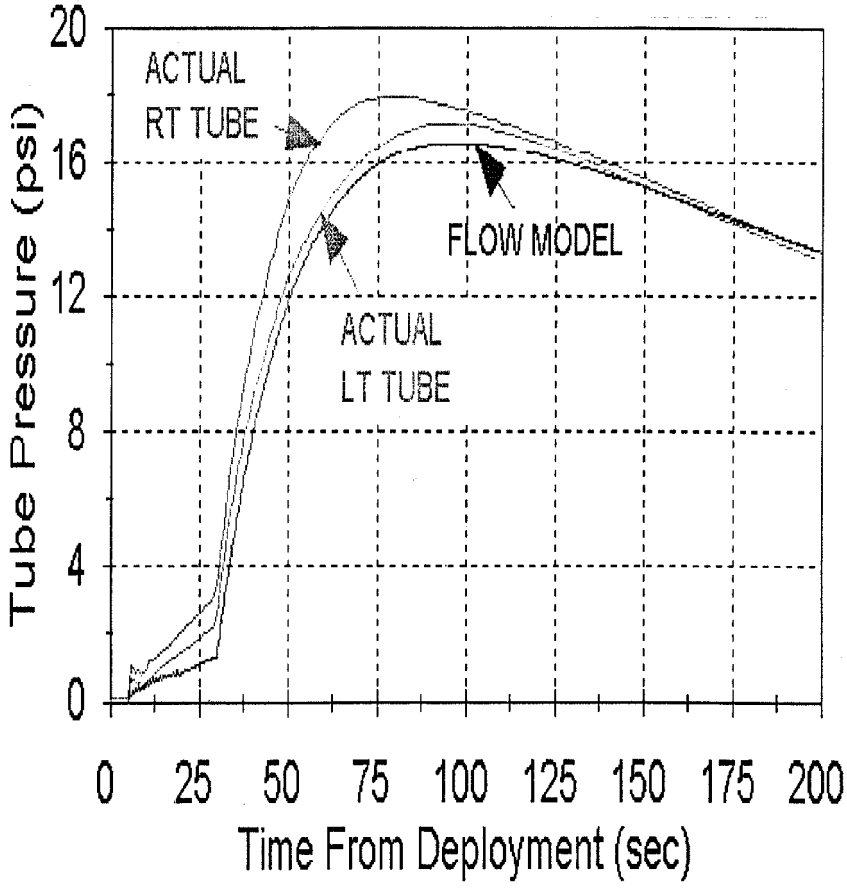

Fig. 8 Influence of the power-law index on the pattern of a) streamlines, b) isotherms, and c) concentration lines (for $Ra = 100$, $Le = 10$, and $N = 5$).

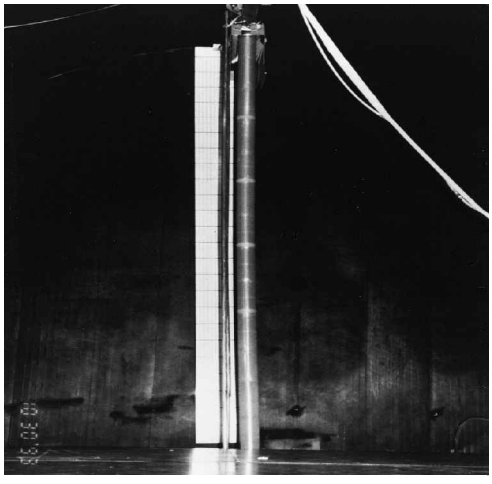

Fig. 9 Variation of the Nusselt number with the buoyancy number: influence of the power-law index ($Ra = 100$ and $Le = 10$).

centration fields plotted in Fig. 5 (for $Le > 1$) and Fig. 6 (for $Le < 1$). These results correspond to the points a and b in Fig. 2, respectively. The streamlines are equally spaced with specified increments, between a value of zero on the boundary and the extreme value. It may be seen from the streamlines (see Figs. 5 and 6) that changing the power-law index modifies the flow structure, at $n > 1$, the entire enclosure is affected by the flow; whereas when $n < 1$, boundary layers appear. This modification of the flow structure has a direct consequence on the concentration fields. This effect can be observed clearly from the results presented in Fig. 6, $Le = 0.1$, which corresponds to point b in Fig. 2. This point corresponds to the flow where $Sh \sim 1$, when the fluid is shear thickening. On the other hand, when the fluid is a shear-thinning fluid, it yields $Sh \sim (L/H)\sqrt[2n]{RaLe}$. Thus, as predicted via scale analysis, at point b the flow has a boundary-layer structure when the fluid is shear-thinning fluid. For the shear-thickening fluids the flow is indeed diffusion dominated. Specifically, our numerical results show that for $n = 1.6$ the concentration lines (see Fig. 6) are parallel to the vertical walls, indicating that most of the mass transfer is by diffusion. As the power-law index decreases, the concentration lines are distorted, which is an indication of the transition from mass transfer dominated by diffusion to mass transfer dominated by convection. Thus, the numerical results in Fig. 6 agree with the trends of the scaling prediction. For heat transfer-driven flow, comparing the streamlines and the isotherms presented in Figs. 5 and 6, as predicted via scale analysis it is seen that the flowfields and the temperature fields are independent of the Lewis number.

For the mass transfer-driven flow, as discussed in the scale-analysis section, the buoyancy is caused primarily by the concentration gradients, i.e., $N > 1$. For this situation, Eq. (35) yields

$$Sh \sim (L/H)(\sqrt[n]{NRaLe})^{1/2} \tag{59}$$

The conclusions that can be drawn from the scale analysis are that the Sherwood number is directly proportional to the buoyancy ratio, the Rayleigh number, and the Lewis number, and it is inversely proportional to the power-law index. Table 3 summarizes the numerical experiments, for $Ra = 100$ and $Le = 10$, performed to document the effect of N and n. As expected, the Sherwood number is clearly seen to increase with increasing N. From the results we can also conclude that, for a fixed value of the buoyancy ratio, the Sherwood number increases with decreasing n. These findings are in agreement

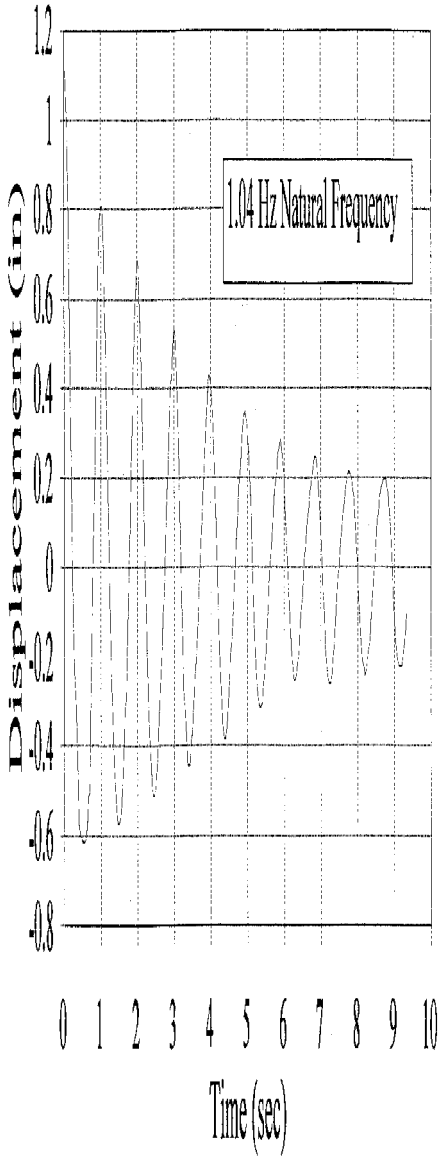

Fig. 10 Vertical velocity profiles in the horizontal midplane at $Ra = 100$, $Le = 10$, and $N = 5$.

with the scaling prediction. The set of results obtained for different values of N and n at $Le = 10$ and $Ra = 100$ are depicted in Table 3 and lead to the following correlation:

$$Sh = 0.6316(\sqrt[n]{NRaLe})^{0.473} \tag{60}$$

where the exponent is in good agreement with the scaling value of 1/2.

Figure 7 shows the numerical results of Table 3, plotted as Sh vs $(\sqrt[n]{NRaLe})$. The analytical solution represented by dashed lines [Eq. (60)], is seen to be in excellent agreement with the numerical solution of the full governing equation, depicted by circles for shear-thickening fluids, filled-circles for Newtonian fluids, and dotted boxes for shear-thinning fluids.

To illustrate the nature of the numerical solution the streamlines, isotherms, and concentration profiles are plotted in Fig. 8 for $Ra = 100$, $Le = 10$, $N = 5$; and $n = 0.5$ (shear-thinning fluids), $n = 1$ (Newtonian fluids), and $n = 1.6$ (shear-thickening fluids). From the results we observe that a significant change in the velocity, concentration, and temperature fields occurs with a change in n. At the given Ra, Le, and N, the shear-thinning fluid ($n = 0.5$) features increased flow circulation within the cavity; thus making the boundary-layer thinner near

Table 2 Numerical results for heat transfer-driven flows[a]

		n			
		1.6		0.5	
Ra	Le	Nu	Sh	Nu	Sh
100.00	10.00	1.56	6.38	22.30	133.20
	100.00	1.56	20.21	22.30	407.02
	500.00	1.56	42.10	22.30	889.21
200.00	10.00	1.99	8.15	42.31	279.88
	100.00	1.99	25.20	42.30	855.01
	500.00	1.99	52.21	——	——
500.00	10.00	2.81	11.30	——	——
	100.00	2.81	34.10	——	——

[a]Average Nusselt and Sherwood numbers.

Table 3 Numerical results for mass transfer-driven flow for $Ra = 100$ and $Le = 10$[a]

	n					
	1.60		1.00		0.50	
N	Nu	Sh	Nu	Sh	Nu	Sh
5.00	1.86	12.40	4.99	34.00	55.01	674.31
10.00	2.21	15.20	6.58	44.81	63.30	1298.72
15.00	2.43	17.21	7.71	56.71	——	——
20.00	2.62	18.81	8.70	64.51	——	——

[a]Average Nusselt and Sherwood numbers.

the two vertical walls and the core fluid more stagnant, as compared with the Newtonian fluid $n = 1$. On the other hand, in the case of the shear-thickening fluid ($n = 1.6$), the flow slows down.

In conclusion, the numerical experiments and scale analysis of the present study provide a balanced description of the phenomenon of natural convection in a porous layer with combined buoyancy effects.

Heat Transfer Results

The overall heat transfer rate of the system under consideration is summarized by resorting to the Nusselt number, defined as

$$Nu = \frac{1}{A}\int_0^A \frac{\partial T}{\partial x}\,\mathrm{d}y \tag{61}$$

In the present analysis the influence of the various input parameters (Ra, Le, N, and n) on the overall behavior of the system is illustrated by plotting graphs of Nu vs the input parameters.

The results presented in the scale-analysis section show that

$$Nu \sim (L/H)(\sqrt[n]{Ra})^{1/2} \tag{62}$$

for heat transfer-driven flow, and

$$Nu \sim \begin{cases} \dfrac{L}{H}(\sqrt[n]{NRa})^{1/2} & \text{if} \quad \delta_T < \delta_C \\ \dfrac{L}{H}\left(\dfrac{\sqrt[n]{NRa}}{Le}\right)^{1/2} & \text{if} \quad \delta_T > \delta_C \end{cases} \tag{63}$$

for the mass transfer-driven flow. Results from the scale analysis predict the overall increase of the average heat transfer caused by the Ra. The results also show that the Nusselt number is independent of the Lewis number in the heat transfer-driven flow. In the mass transfer-driven flow, Nu varies with the Lewis number when $\delta_T < \delta_C$. Furthermore, Eqs. (62) and (63) predict an increase of the Nusselt number when decreasing the power-law index. Observation of the numerical results

presented in Tables 2 and 3 confirm the predictions made by the scale analysis. A view of the heat transfer within a porous layer heated from the side is given in Fig. 9, where the numerically determined overall Nusselt number Nu is plotted as a function of N and n. Figure 9 indicates that Nu increases monotonically when increasing N in all power-law fluids considered herein. Here again it appears clearly that for a fixed value of N the Nusselt number increases as n decreases. This is because the apparent viscosity is reduced with a shear rate increase.

The influence of the power-law index on the average heat transfer implies that the convective transport of heat increases with decreasing n. Figure 6 for the heat transfer-driven flow and Fig. 8 for the mass transfer-driven flow exemplify this prediction by showing a significant change in the velocity, temperature, and concentration fields with a change in the power-law index. As discussed in the preceding section the results showed that decreasing the power-law index results in strengthening the flow circulation within the cavity. This is well illustrated by the vertical velocity profiles in the horizontal midplane (Fig. 10) for $n = 0.5$, 1.0, and 1.6 at $Ra = 100$, $Le = 10$, and $N = 5.0$, respectively. The profiles clearly show that the velocity maximum increases, and the thickness of the corresponding boundary layer decreases, with decreasing n. Stronger convection, for shear-thinning fluids, results in turn in enhanced heat transfer, which is in agreement with the scaling prediction.

Conclusions

Using the modified Darcy model of Pascal,[14] we examined the steady double diffusion in a rectangular cavity saturated with a non-Newtonian fluid. The effect of the major system parameters (Ra, Le, N, and n) on the double-diffusion phenomenon has been investigated in two different manners: numerically and by using a scaling approach. These two methods provide a balanced description of the phenomenon of double diffusion in a porous layer. The numerical results support the trends and flow regimes predicted by the theoretical order-of-magnitude analysis. The scale analysis, on the other hand, successfully sorted out the many effects that influence the outcome of the discrete numerical experiment.

Summarizing the results of the analytical and numerical analyses, the following conclusions can be drawn. The average Sherwood and Nusselt numbers are found to be sensitive to the Rayleigh number, Lewis number, buoyancy ratio, and the power-law index of the fluids. The power-law index is observed to influence the flow, temperature, and concentration fields significantly. Compared to the Newtonian fluids, a decrease in the power-law index (shear-thinning fluids) enhances the convection heat and mass transfer while an increase in the power-law index (shear-thickening fluids) yields corresponding reductions. In the case of heat transfer-driven flow ($N = 0$) for the non-Newtonian fluids with different power-law indexes, the heat transfer results are independent on the Lewis number. The mass transfer results, however, depend on Le.

References

[1]Nield, D. A., and Bejan, A., *Convection in Porous Media*, Springer–Verlag, New York, 1992.

[2]Trevisan, O. V., and Bejan, A., "Natural Convection with Combined Heat and Mass Transfer Buoyancy Effects in a Porous Medium," *International Journal of Heat and Mass Transfer*, Vol. 28, No. 8, 1985, pp. 1597–1611.

[3]Trevisan, O. V., and Bejan, A., "Combined Heat and Mass Transfer by Natural Convection in a Porous Medium," *Advances in Heat Transfer*, Vol. 20, Academic, New York, 1990, pp. 315–352.

[4]Alavyoon, F., "On Natural Convection in Vertical Porous Enclosure Due to Prescribed Fluxes of Heat and Mass at the Vertical Boundaries," *International Journal of Heat and Mass Transfer*, Vol. 36, No. 10, 1993, pp. 2479–2498.

[5]Alavyoon, F., Masuda, Y., and Kimura, S., "On Natural Convection in Vertical Porous Enclosures Due to Opposing Fluxes of Heat and Mass Prescribed at the Vertical Walls," *International Journal of Heat and Mass Transfer*, Vol. 37, No. 2, 1994, pp. 195–206.

[6]Goyeau, B., Songbe, J. P., and Gobin, D., "Numerical Studies of Double-Diffusive Natural Convection in a Porous Cavity Using the Darcy-Brinkman Formulation," *International Journal of Heat and Mass Transfer*, Vol. 39, No. 7, 1996, 1363–1378.

[7]Bird, R. B., Armstrong, R. C., and Hassger, O., *Dynamics of Polymeric Liquids*, Vol. 1, Wiley, New York, 1987.

[8]Crochet, M. J., Davies, A. R., and Walters, K., *Numerical Simulation of Non-Newtonian Flow*, Elsevier, New York, 1987.

[9]Chhabra, R. P., *Bubbles, Drops and Particles in Non-Newtonian Fluids*, CRC Press, London, 1993.

[10]Bian, W., Vasseur, P., and Bilgen, E., "Boundary-Layer Analysis for Natural Convection in a Vertical Porous Layer Filled with a Non-Newtonian Fluid," *International Journal of Heat and Fluid Flow*, Vol. 15, No. 5, 1994, pp. 384–391.

[11]Bian, W., Vasseur, P., and Bilgen, E., "Natural Convection of Non-Newtonian Fluids in an Inclined Porous Layer," *Chemical Engineering Communication*, Vol. 129, 1994, pp. 79–97.

[12]Getachew, D., Minkowycz, W. J., and Poulikakos, D., "Natural Convection in a Porous Cavity Saturated with Non-Newtonian Fluid," *Journal of Thermophysics and Heat Transfer*, Vol. 10, No. 4, 1996, pp. 640–651.

[13]Rastogi, S. K., and Poulikakos, D., "Double-Diffusion from a Vertical Surface in a Porous Region Saturated with a Non-Newtonian Fluid," *International Journal of Heat and Mass Transfer*, Vol. 38, No. 5, 1995, pp. 935–946.

[14]Pascal, H., "Rheological Behavior Effect of Non-Newtonian Fluids on Steady and Unsteady Flow Through Porous Media," *International Journal of Numerical and Analytical Mechanics in Geomechanics*, Vol. 7, No. 3, 1983, pp. 289–303.

[15]Bejan, A., *Convection Heat Transfer*, Wiley, New York, 1984.

[16]Patankar, S. V., *Numerical Heat Transfer and Fluid Flow*, Hemisphere, Washington, DC, 1980.

[17]Patankar, S. V., *Computation of Conduction and Duct Flow Heat Transfer*, Innovative Research, Inc., Maple Grove, MN, 1991.

[18]Patankar, S. V., "Elliptic Systems: Finite Difference Method I," *Handbook of Numerical Heat Transfer*, edited by W. J. Minkowycz, E. M. Sparrow, G. E. Schneider, and R. H. Pletcher, Wiley, New York, 1988, pp. 215–240.

[19]Walker, K. L., and Homsy, G. M., "Convection in a Porous Cavity, *Journal of Fluid Mechanics*," Vol. 87, Pt. 3, 1978, pp. 449–474.